

# Tectonics

## RESEARCH ARTICLE

10.1029/2020TC006181

### Key Points:

- A regional seismic data interpretation in the Great South Basin revealed three stages of fault evolution over about 22 Ma
- Dominant fault set trends NE and minor fault set trends NW, with the latter forming along basement terrane boundaries
- Rift faulting is interpreted to reflect the embryonic stages of Gondwana breakup

### Supporting Information:

- Supporting Information S1
- Figure S1
- Figure S2
- Figure S3

### Correspondence to:

T. R. Sahoo,  
t.sahoo@gns.cri.nz

### Citation:

Sahoo, T. R., Nicol, A., Browne, G. H., & Strogen, D. P. (2020). Evolution of a normal fault system along eastern Gondwana, New Zealand. *Tectonics*, 39, e2020TC006181. <https://doi.org/10.1029/2020TC006181>

Received 2 MAR 2020

Accepted 8 SEP 2020

Accepted article online 15 SEP 2020

## Evolution of a Normal Fault System Along Eastern Gondwana, New Zealand

T. R. Sahoo<sup>1,2</sup> , A. Nicol<sup>2</sup> , G. H. Browne<sup>1</sup> , and D. P. Strogen<sup>1</sup> 

<sup>1</sup>GNS Science, Lower Hutt, New Zealand, <sup>2</sup>School of Earth and Environment, University of Canterbury, Christchurch, New Zealand

**Abstract** The Great South Basin (GSB) developed in the Cretaceous from continental rifting at the southeastern margin of Gondwana. The basin contains a thick Cretaceous succession that is largely unaffected by Neogene compressional tectonics, with rift faults and associated growth strata imaged by good-quality 2-D and 3-D seismic data tied to wells. These data show three distinct stages of normal faulting here referred to as fault system initiation (Stage 1), fault system growth (Stage 2), and fault system death (Stage 3). The different stages of fault system evolution comprise dominant NE trending faults (NW-SE extension), and minor NW trending faults (NE-SW extension). Fault initiation at ~105–101 Ma mainly occurred in the central GSB with rift depocenters mostly on, or close to, NW trending basement terrane boundaries. These preexisting basement boundaries represent zones of weakness that locally promoted early localization of NW faults and retarded the propagation of NE faults. With increasing regional extension and fault system growth from ~101 to 90 Ma the influence of the basement fabric gradually decreased, while NE trending faults increased in length, number, displacements, and spatial distribution. Finally, during the fault system death stage from ~90 to 83 Ma the length, number and displacements of faults decreased. Fault death coincided in time with Gondwana breakup and reflects the localization of extension along spreading centers distal to the GSB.

## 1. Introduction

Rift basins form due to extensional tectonics, with the growth histories of faulting providing insights into continent-scale processes. In ancient rift systems normal faults initiate, grow and die (e.g., Childs et al., 2003; Meyer et al., 2002; Nicol et al., 2020; Walsh et al., 2002), however, in many cases the detailed evolution of fault systems is unknown. Faulting in rift basins that were subject to erosion of growth strata during basin inversion and/or uplift are particularly poorly resolved (Bull et al., 2019; Davison & Underhill, 2012; King & Thrasher, 1996). The resulting incompleteness of basin fill growth strata is common for the late stages of faulting and little has been published about how normal faults die (Nicol et al., 2020). To resolve these completeness issues, we study Cretaceous faulting in the Great South Basin (GSB) in offshore southeastern New Zealand, where the rift sedimentary succession and history of faulting are well imaged in seismic reflection profiles. Therefore, the GSB is an ideal location to study fault evolution and provide insights to a number of key questions including: How do fault systems evolve through space and time? How does the fault evolution relate to Gondwana breakup and what are the implications for the evolution of Southern Zealandia?

The GSB is one of several continental rift basins that formed during mid-Cretaceous (~105 Ma) extension at the eastern margin of Gondwana (Beggs, 1993; Cook et al., 1999; Grobys et al., 2009; Kula et al., 2009; Laird, 1993; Laird & Bradshaw, 2004; Strogen et al., 2017; Sutherland et al., 2001; Uruski et al., 2007). Crustal thinning and extension in the GSB formed in association with fragmentation of eastern Gondwana and the ultimate formation of the Zealandia continent (Adams et al., 2017; Bache et al., 2014; Davy, 1993, 2014; Eagles et al., 2004; Grobys et al., 2007, 2008; Luyendyk, 1995; Luyendyk et al., 1996, 2003; Mortimer et al., 2019; Uruski et al., 2007). The rifting studied here primarily predates the formation of the spreading centers surrounding Zealandia and is thought to have formed as part of the preseparation stage of the Gondwana breakup process (Barrier, 2019; Siddoway et al., 2004; Spell et al., 2000; Strogen et al., 2017). The resulting normal faults have been preserved to the present day in part due to latest Cretaceous and Paleogene passive drift and associated subsidence. In this paper we use 2-D and 3-D seismic reflection lines (tied to petroleum wells) to examine the geometries, displacement histories, and growth of

normal faults that formed during the mid-Cretaceous to Paleocene (~105 to 56 Ma) in the GSB. These data allow us to establish the evolution of a regional-scale fault system from its inception, as it matures and then eventually dies. This study has implications for fault system evolution in regions with strong basement fabrics, for the geological evolution of Southern Zealandia and for Gondwana breakup.

## 2. Geological Setting

The GSB is a mid-Cretaceous and younger sedimentary basin located southeast of New Zealand. The basin formed on the continental crust of Zealandia which comprises basement rocks of Paleozoic and Mesozoic age that were part of the paleo-Pacific eastern Gondwana margin (Figure 1; Mortimer et al., 2017). Basement rocks in Zealandia comprise a series of metasedimentary tectonostratigraphic terranes (Takaka, Buller, Torlesse Composite, Brook Street, Murihiku, Caples, Waipapa, and Dun Mountain-Maitai), their metamorphosed equivalents (Haast Schist), and the median batholith magmatic arc (Bradshaw, 1989; Mortimer et al., 1999; Muir et al., 1994, 1995; Tulloch & Kimbrough, 2003; Tulloch et al., 2019). These terranes are exposed in the eastern South Island where they trend NW-SE and based on deep-crustal seismic lines and well data are inferred to extend offshore with similar trends beneath the Great South and Canterbury basins (Barrier et al., 2018; Field et al., 1989; Mortimer, 2004; Mortimer et al., 1999, 2014). Onshore these terranes produce a heterogeneous basement, with the terrane boundaries typically defined by crustal-scale Mesozoic faults generated during the terrane accretion process (Bradshaw, 1989; Mortimer, 2004; Mortimer et al., 2002, 2014; Muir et al., 2000; Phillips & McCaffrey, 2019; Tarling et al., 2019).

The middle to Late Cretaceous geological history of New Zealand involved continental breakup of Gondwana and separation of the Zealandia continent from Australia and Antarctica (Gaina et al., 1998; Kula et al., 2009; Mortimer et al., 2014, 2017). The rocks and sediments formed on the Zealandia continent after the Gondwana breakup and/or during the rifting phase are termed the Zealandia Megasequence (Mortimer et al., 2014). Breakup was preceded by regional extension, crustal thinning, subsidence, and the formation of sedimentary basins, with rifting of the Gondwana margin recognized widely throughout Zealandia and most often inferred to date from ~105 to 83 Ma based on analysis of onshore and offshore sediments (Strogen et al., 2017, and references therein). By the Late Cretaceous (~83–79 Ma) seafloor spreading was well established in the South Pacific, and New Zealand drifted away from both Antarctica and Australia (Gaina et al., 1998; Strogen et al., 2017). This drift reflected a period of postrift thermal subsidence and sag in the GSB (Constable & Crookbain, 2011; Cook et al., 1999; Sahoo, King, et al., 2014). From the latest Cretaceous, the post breakup succession was marked by passive drift tectonics, with the GSB largely unaffected by the Neogene tectonics that deformed much of New Zealand by Alpine Fault movement and subduction of the Hikurangi margin further to the north (Cooper et al., 1987; Nicol et al., 2007; Sutherland, 1995).

Previous publications in the GSB using seismic reflection and well data have identified steeply moderately dipping faults striking mainly NE with subordinate NW striking faults (Constable & Crookbain, 2011; Cook et al., 1999; Sahoo, King, et al., 2014). Recently, the geometric and kinematic evolution of faults have been described in and around the GSB-3D seismic reflection area in the southern GSB (Phillips & McCaffrey, 2019). However, detailed analysis of fault geometries and evolution has not been previously undertaken on a regional scale in the GSB. The present paper builds on the previous work and focuses regional-scale analysis of fault growth to understand the spatial and temporal evolution of a normal fault system.

## 3. Data and Methods

The GSB has been selected in this study because (1) it contains a thick Cretaceous sedimentary succession ~7 km thick providing an expanded record of tectonosedimentary relationships, (2) basin strata and faulting are well imaged by high-quality and regionally extensive 2-D seismic reflection data and localized 3-D seismic reflection data, (3) the age and correlation of basin strata is constrained by eight open-file petroleum exploration wells tied to seismic lines, and (4) first-order sedimentological and biostratigraphical control for the observed sedimentary basin fill is well documented in previous publications (Beggs, 1993; Cook et al., 1999; Sahoo & Bland, 2017; Schiøler & Raine, 2009; Schiøler et al., 2017; Sutherland et al., 2001).

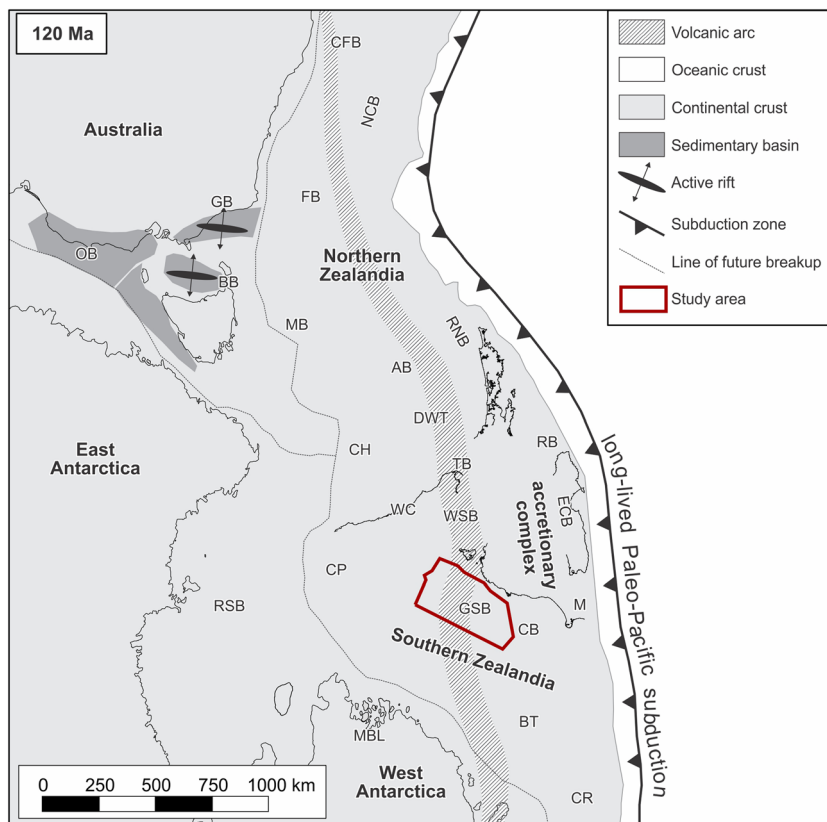


**Figure 1.** A regional reconstruction showing the position of northern and southern Zealandia in eastern Gondwana at ~120 Ma (modified after Strogen et al., 2017). The positions of major structural features and sedimentary basins are shown, with the GSB outlined by the red polygon. Abbreviations used: GSB = Great South Basin; CR = Chatham Rise; BT = Bounty Trough; CB = Canterbury Basin; M = Marlborough; CP = Campbell Plateau; RS = Ross Sea; WSB = Western Southland Basin; WC = West Coast basins; TB = Taranaki Basin; ECB = East Coast Basin; CH = Challenger Plateau; RB = Raukumara Basin; DWT = Deepwater Taranaki; AB = Aotea Basin; RNB = Reinga–Northland Basin; MB = Monawai Basin; BB = Bass basins; OB = Otway Basin; GB = Gippsland Basin; FB = Fairway Basin; NCB = New Caledonia Basin; CFB = Capel–Faust Basin; MBL = Marie Byrd Land.

Two-dimensional seismic lines totalling >58,000 line kilometers cover most parts of the basin (Figure 2). These seismic lines were collected from 1971 to 2015 and the data quality is variable. Recently acquired (post-2000) or reprocessed 2-D seismic surveys are of very good quality. They cover the central and northeastern parts of the GSB with line spacing 0.5–7 km, while 2-D seismic line spacing in the southern and northwestern part of the GSB are typically 6–36 km (Figure 2) (for further details of the seismic surveys see Sahoo, King, et al., 2014). In addition, two 3-D seismic surveys, GSB-3D ( $1,344 \text{ km}^2$ ; CGGVeritas, 2009) and Rigel-3D ( $4,880 \text{ km}^2$ ; Shell GSB Ltd, 2013) are available in the GSB (Figure 2). Horizon and fault interpretation were carried out for 2-D and 3-D seismic data using Paradigm software to develop cross sections, structure contour and stratigraphic thickness maps, and fault displacement profiles. Interpretations of seismic lines and displacement analysis were performed in the time domain. Horizon grids were converted from time to depth for thickness estimation using the velocity model of Sahoo and Bland (2017).

The Cretaceous-Paleocene succession (Figure 3) is the primary focus of this study. Seven regional seismic horizons (Basement, K40, K65, K80, K90, P00, and P10; horizon names use the nomenclature of Strogen & King, 2014) were interpreted on open-file 2-D and 3-D seismic surveys (e.g., Figure 3). These horizons were interpreted to map different wedge-like depositional growth packages within the rift-succession and to understand the temporal evolution of faulting. The basement horizon marks the base of mid-Cretaceous rift strata within grabens of the offshore GSB. Horizons K40, K65, and K80 represent the top of wedge-like depositional packages above basement. In general, these horizons form unconformities

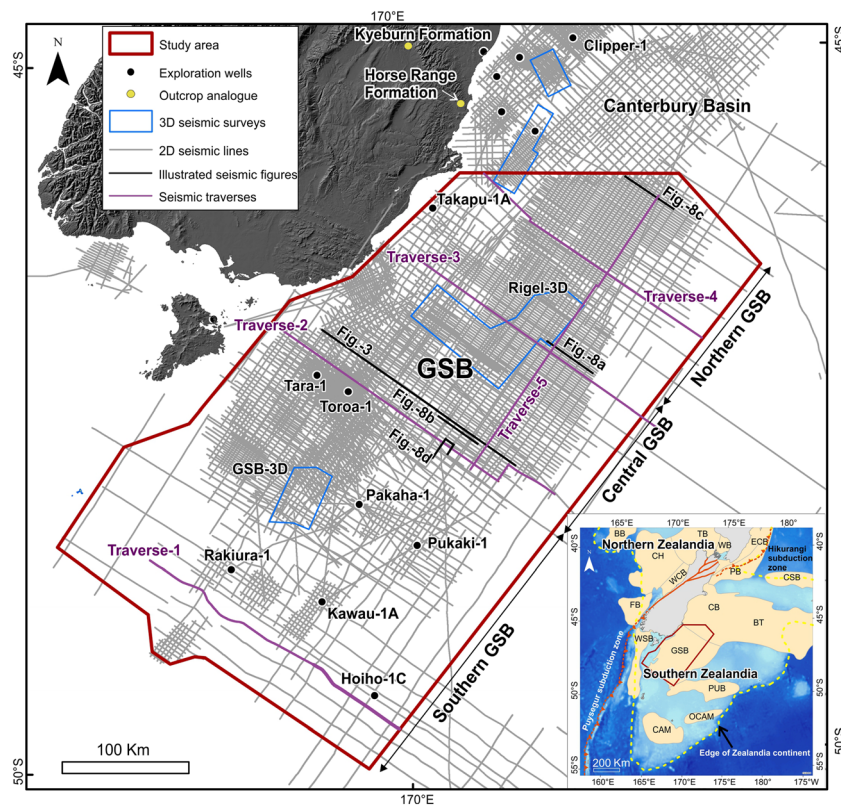


**Figure 2.** Base map of the GSB showing study area, open file 2-D/3-D seismic data, 3-D surveys and exploration wells. Onshore outcrops of the mid-Cretaceous Kyeburn and Horse Range formations are also indicated. Crustal stretching was estimated along the four traverses (1–4). Seismic lines illustrated in later figures are also shown. The inset map shows the location of the GSB (red polygon) with respect to other Zealandia basins (see Figure 1). Abbreviations used in the inset map: PB = Pegasus Basin; CSB = Chatham Slope Basin; WCS = West Coast Basin; PUB = Pukaki Basin; OCAM = outer Campbell Basin; CAM = Campbell Basin. See Figure 1 caption for other abbreviations.

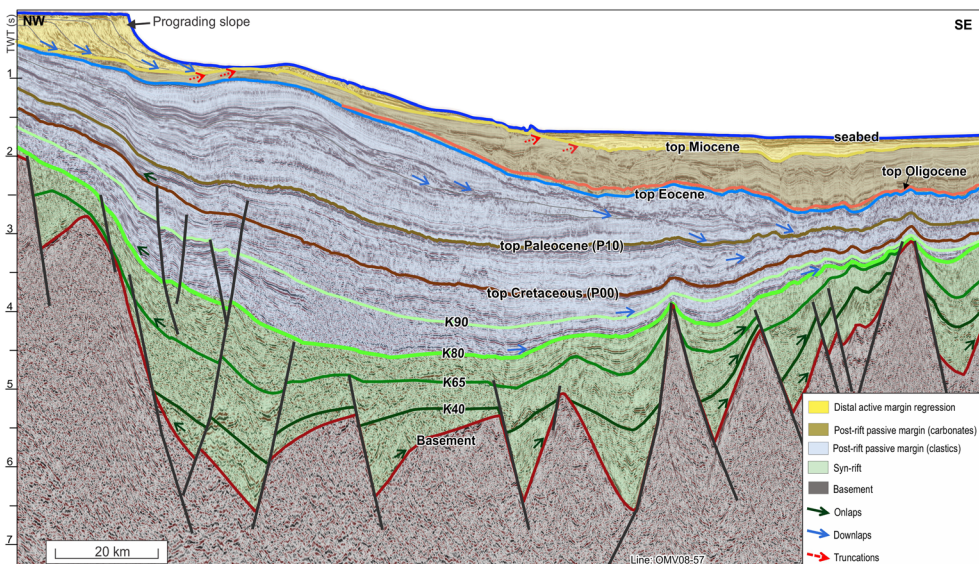


**Figure 3.** Regional seismic section showing major interpreted horizons and regional tectonostratigraphic units in the GSB. Four major sequences within the Cretaceous to Neogene succession such as synrift, postrift passive margin (clastics), postrift passive margin (carbonates), and distal active margin regression are recognized. Reflection terminations (onlaps, downlaps, and truncations) are shown as arrows. See Figure 2 for location.

across structural highs. The seismic unit above the K80 horizon has continuous seismic reflectors that onlap basin margins and record marine transgression into the basin. Horizon K90 is interpreted to be a transgressive surface mapped between the K80 and P00. Horizon P00 and P10 represent the top of the Cretaceous and the Paleocene successions, respectively. These horizons were assigned an age using biostratigraphy established from 14 offshore wells (Blanke, 2015; Hunt International Petroleum Co NZ, 1977a, 1977b, 1977c, 1978a, 1978b, 1978c; Placid Oil Company, 1984a, 1984b; Schiøler & Raine, 2009; Schiøler et al., 2011, 2012, 2017). Of these wells, eight were located in the GSB and six to the northeast in the contiguous Canterbury Basin (Figure 2). Checkshot information of these wells were used to tie wells to seismic data; details of the well-seismic ties in the GSB are described in Sahoo, King, et al. (2014).

The oldest sedimentary rocks in the offshore GSB were penetrated in the well Kawau-1A (Figure 2) and in the offshore Canterbury Basin in the well Clipper-1 (Figure 2) and are of late Motuan New Zealand Stage age (~100 Ma; Raine et al., 2018; Schiøler & Raine, 2009; Schiøler et al., 2011). These wells were drilled on structural highs and the oldest sedimentary rocks in adjacent grabens could be older. The age of the oldest sedimentary strata is provided by geochronological ages of ~112 Ma from volcanic rocks onshore (Shag Valley Ignimbrite in Horse Range Formation and Eweburn Tuff in Kyeburn Formation; Tulloch et al., 2009; Figure 2), while biostratigraphic information from these rock outcrops indicate ages of ~117–108 Ma (Schiøler & Raine, 2009). These strata are considered to be prerift sedimentary rocks formed in association with arc volcanism (Tulloch et al., 2019). However, due to poor exposure of these outcrops and lack of seismic data in this region, the timing of deposition of these outcrop strata relative to the onset of faulting remains unclear and, consistent with previous publications (Crampton et al., 2019; Laird, 1993; Sutherland et al., 2001), we adopt ~105 Ma as the onset of faulting (here inferred to be equivalent to the top basement horizon). The ages of the K40, K65, K80, K90, P00, and P10 horizons adopted in this publication were estimated by correlation to offshore wells (e.g., Kawau-1A, Hoiho-1C, Pukaki-1, Pakaha-1, Rakiura-1, Tara-1, Toroa-1, Galleon-1, Cutter-1, Endeavour-1, Clipper-1, and Caravel-1). The ages of the interpreted horizons (i.e. Basement = ~105 Ma, K40 = ~101 Ma, K65 = ~90 Ma, K80 = ~83 Ma, K90 = ~75 Ma, P00 = ~66 Ma, and P10 = ~56 Ma) are considered to be within error margin of  $\pm 1\text{--}3$  Myr and are shown on the summary stratigraphic column for the GSB in Figure 4. Uncertainties on horizon ages may impact the estimated timing of faulting, but they do not impact the relative timing of displacement accumulation on individual faults or the relative timing of fault growth across the basin.

Faults with vertical displacement of  $>10$  ms (milliseconds) two-way travel time (TWT) were mapped in the GSB using 2-D and 3-D seismic lines. In this regional study, only faults with lengths  $>5$  km have been included in the fault map. Fault displacements in TWT provide first-order information on fault growth. Fault surfaces (350 faults) were generated where the same fault can be mapped in more than one seismic line. These surfaces were used to characterize fault geometries. For 2-D data the locations of fault tips beyond existing seismic lines were estimated using fault displacement gradients along the fault strike. Coherency cubes derived from 3-D seismic data were also used to define faults within these volumes. For both 2-D and 3-D average fault trends were inferred to be parallel to the trend of the line joining the end points of each fault trace. These trends, which are here inferred to parallel average fault strike, were estimated at multiple stages of fault growth.

Fault growth is preserved by up-sequence decreases in displacement in the rift sequence growth strata (e.g., Childs et al., 2003; Nicol et al., 2020). Fault vertical displacements (or throws) were measured in TWT between horizon cut-offs on fault footwalls and the hangingwall on up to seven horizons for individual faults in seismic sections. On some of the larger faults, footwall horizons onlap structural highs and, in these cases, fault throw was estimated using the TWT of the projected reflector terminations in the fault footwall and the hangingwall cut-off (Figure 5). The impact of compaction on displacement is considered to be relatively minor (<20% of the total displacement, Taylor et al., 2008) and the decompression likely does not affect the first-order throw patterns measured in this study. Therefore, the faulted strata were not decompacted in this regional-scale study. The resulting displacement data have been used to generate along-strike throw profiles for individual horizons (Figure 5b) and dip profiles showing variations in displacement up-sequence. Fault displacement history plots were developed using displacement measurements from individual seismic lines in conjunction with the displacement backstripping technique. In the displacement backstripping method vertical displacement on successively older horizons is sequentially subtracted from all

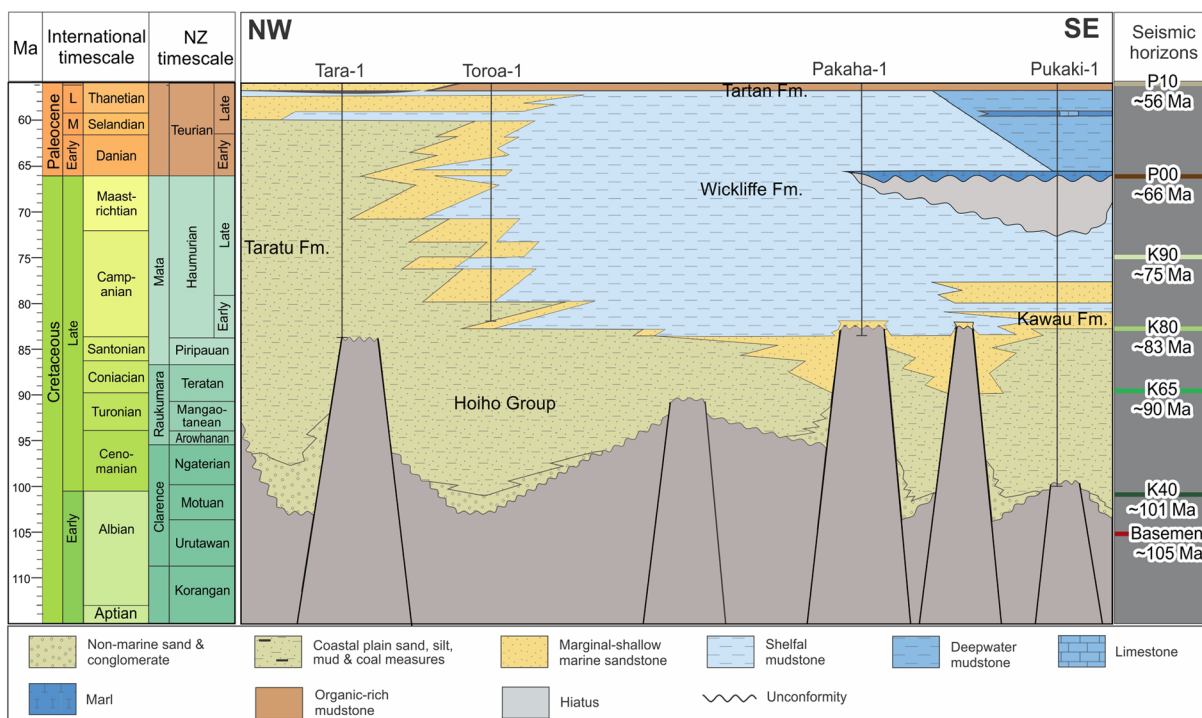


**Figure 4.** Generalized chronostratigraphic framework of the GSB, showing major lithostratigraphic units and ages of interpreted seismic horizons (modified after Constable & Crookbain, 2011; Cook et al., 1999; Schiøler & Raine, 2009). See Cook et al. (1999) for further details on lithostratigraphy.

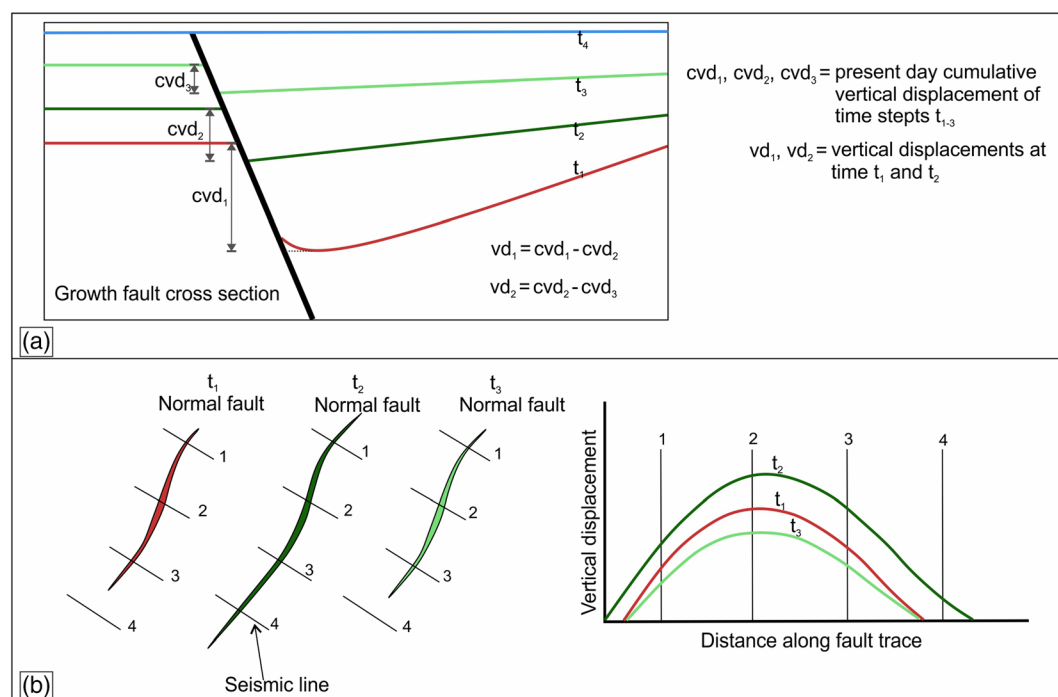


**Figure 5.** (a) Method for estimating vertical displacement at different time steps using displacement backstripping (modified after Reilly et al., 2015). (b) Fault displacement measurements along the fault trace (modified after Reilly et al., 2015).

underlying horizons (Childs et al., 1993; Giba et al., 2010; Reilly et al., 2015). Fault displacement history plots were constructed to show the accumulation of displacement during deposition of the growth sequence for 35 faults (see more details in Figure 10 in section 5). In addition, we use displacement backstripping of multiple seismic lines across individual faults to determine changes in fault length through time. A cartoon outlining the backstripping method to estimate increments of vertical displacement and fault propagation is shown in Figure 5.

Extension across the GSB was estimated using fault heaves along five regional traverses (Figure 2). Cumulative fault heaves at different stratigraphic levels (~105, 101, 90, 83, and 75 Ma) have been measured in four seismic traverses oriented NW-SE and one traverse oriented NE-SW (Figure 2) to understand the spatial and temporal distribution of crustal stretching. Extension on younger horizons were sequentially subtracted from extension on older horizons to estimate the incremental extension for ~105, 101, 90, 83, and 75 Ma time steps along the seismic traverses selected. The amount of extension and the length of the traverse prior to stretching at different times were used to estimate the percentage of extension for the time intervals listed. The amount of extension estimated across interpreted faults are minimums as this method does not include extension on subseismic scale faults not observed in our data (e.g., Walsh et al., 1991). Despite these sampling issues, the extension data can be used to provide regional-scale information on the evolution of faulting in the GSB. While these do not present absolute estimates of extension, they are internally consistent and can be compared relative to other transects across the GSB.

#### 4. Geometries, Displacements, and Timing of Faulting

Cretaceous normal faults in the GSB show cumulative vertical displacements up to 3,000 ms (~4,500 m) and lengths up to ~110 km (Figure 6b). Faults display a range of fault strike, dip direction, and dip angle (~25° to 50°). They form horst and graben structures with a component of normal dip-slip (Figure 3). The faulting pattern is characterized by active normal faults with growth strata on the downthrown side and show widespread development of grabens and half-grabens. The fault system comprises two main fault sets, with dominant NE (30–70°) and subordinate NW (300–315°) strikes (Figures 6 and 7). The normal faults that bound major grabens and half-grabens trend parallel to the dominant fault sets. These grabens are filled with up to ~4,500 m of synfaulting strata. In the central and southern GSB (Figure 2) the thickness of growth strata is typically roughly equal to fault displacements, suggesting that in these regions, sediment supply filled the available accommodation space created by faulting. However, in the northern GSB some depocenters are underfilled (Figure 8c) where the thickness of growth strata (Basement-K80) is less than the accommodation space created by faulting. Individual grabens are 5–30 km wide in the central and southern areas and 5–20 km wide in the northern areas. The length of the faults and associated grabens varies from 5 km to >100 km. Longer faults (>100 km) are developed in the central and southern regions, while the longest fault mapped in the northern area is around 75 km. NE striking faults are widespread throughout the GSB and Canterbury Basin (Barrier, 2019; Barrier et al., 2020; Sahoo, Browne, & Hill, 2014; Sahoo, King, et al., 2014; Sahoo, Kroeger, et al., 2015) and trend subparallel to the eastern margin of Southern Zealandia. NW striking faults are locally subparallel to the Mesozoic basement terrane boundaries (Barrier, 2019; Sahoo, King, et al., 2014). Despite the varying trends, the fault geometries and displacements of both fault sets are characteristic of extension, with little evidence of strike-slip. Maximum displacements and lengths are typically greater for NE trending faults (up to 3,000 ms displacement and up to ~110 km length) as opposed to NW trending faults (up to ~2,000 ms displacement and up to ~40 km length).

Extension and normal faulting in the GSB primarily occurred between ~105 and 83 Ma, predating the breakup of Gondwana (Figures 6 and 7). A minor set of faults (Figure 6) with small displacements were also observed post 83 Ma (see details in section 5); however, these faults contribute <5% to the rift related extension. The timing of normal faulting is consistent with the age of extension in many other basins underlain by Zealandia continental crust (see Strogen et al., 2017, and references therein). The four mapped seismic horizons within the growth sequence (i.e., top basement, K40, K65, and K80) provide a basis for analyzing the details of fault growth during three stages (Figures 6 and 8). These stages are here referred to as: Stage 1: fault system initiation (between top basement and K40 horizons and ~105–101 Ma), Stage 2: fault system growth (between K40 and K65 horizons and ~101–90 Ma), and Stage 3: fault system death (between K65 and K80 horizons and ~90–83 Ma). A similar fault growth

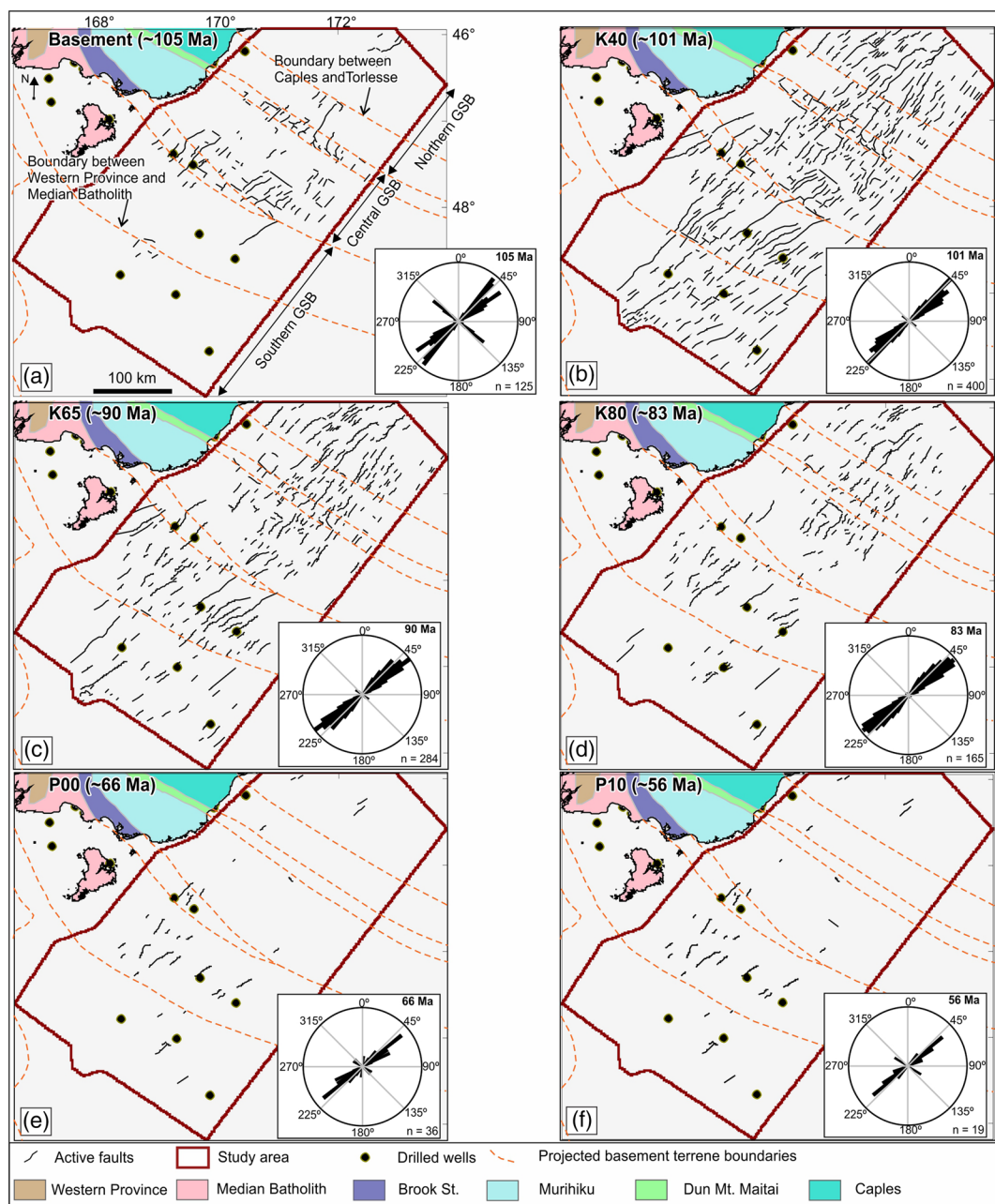


**Figure 6.** Maps of active faults and rose diagrams summarizing fault orientations at ~105, 101, 90, 83, 66, and 56 Ma. Basement terrane boundaries in the onshore areas are adopted from Mortimer et al. (2012) (see references therein for detailed information on onshore basement terranes). The projected basement boundaries in the offshore GSB are shown as orange dash lines (modified after Constable & Crookbain, 2011; Tulloch, 2010).

model (particularly the early two stages of fault evolution) was also described from a number of other basins by Gawthorpe and Leeder (2000). Each faulting episode shows major fault displacements at the base of each unit (Figure 8). The faulting episodes are separated by unconformities at structural highs and show onlapping reflection patterns onto the base of the interval (Figure 8). It is assumed that these unconformities were developed by footwall uplift, erosion, and nondeposition induced by faulting (after a model for synrift accommodation development by Ravnås & Steel, 1998). Below we discuss the growth of faults and the fault system during each stage of faulting.

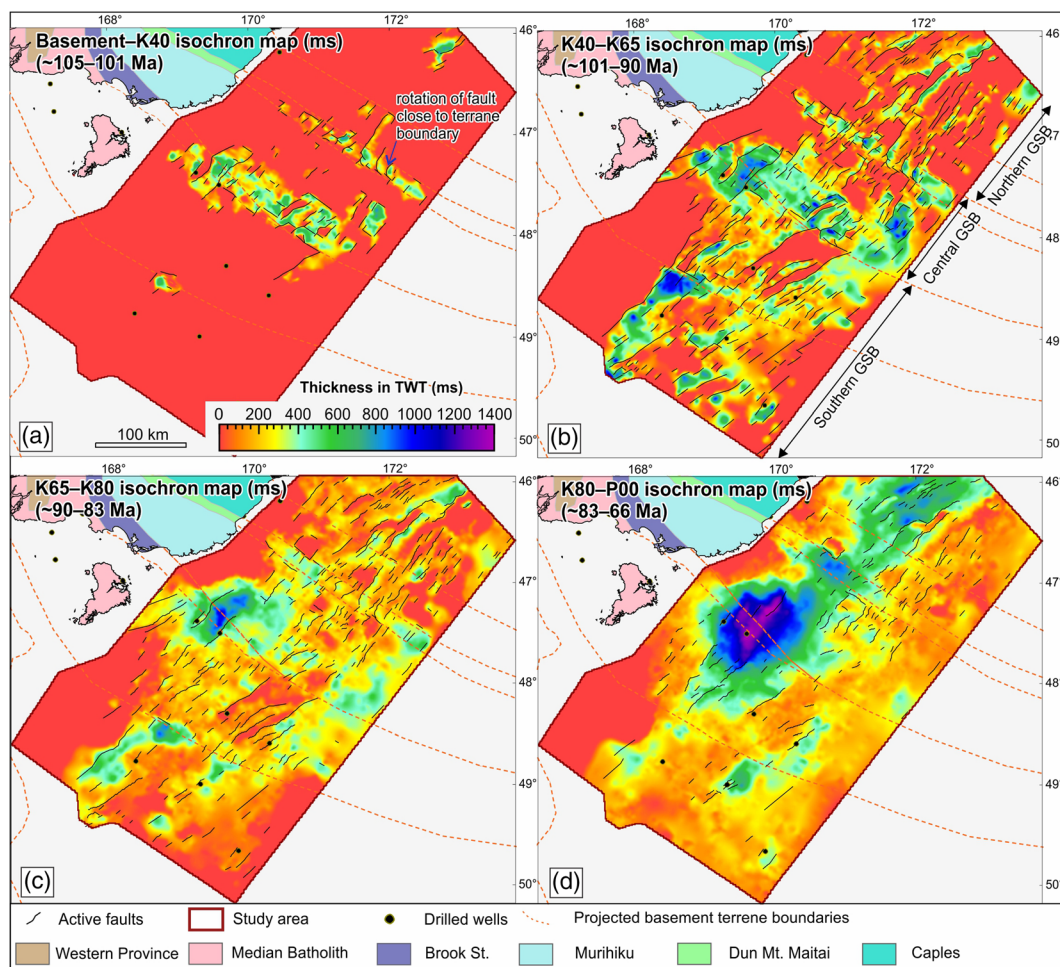


**Figure 7.** (a) Isochron map of the interval Basement-K40 (~105–101 Ma; first stage of faulting). (b) Isochron map of the interval K40-K65 (~101–90 Ma; second stage of faulting). (c) Isochron map of the interval K65-K80 (~90–83 Ma; third stage of faulting). (d) Isochron map of the interval K80-P00 (~83–66 Ma). Black lines show active faults at base of each isochron map. Basement terrane boundaries are also indicated. The TWT structure maps that were used to derive these isochron maps are provided as supporting information Figures S1 and S2. Isochron map between P00-P10 interval is provided as supporting information Figure S3.

## 5. Faulting History

### 5.1. Stage 1—Fault System Initiation

Thickening of growth strata indicate that both NE and NW trending faults were active during the first stage of faulting, which occurred between ~105 and 101 Ma. Relatively few active faults ( $N = 125$ ) have been interpreted as active at ~105 Ma with a short aggregate fault length of ~1,650 km (i.e., average fault length of ~13 km) (Figures 6a, 7a, and 9a). These faults produced a series of isolated grabens and half-grabens mainly in the central GSB containing up to ~700 ms of strata (~1,400 m thickness; Sahoo & Bland, 2017). NE trending grabens were most common, although some tectonic depressions were bound by both NE and NW trending faults. At this early stage of extension NE trending faults dominate (89 of 125 faults or ~70% trend NE) and most of the longer faults in the system trend NE and dip SE. The NW trending faults (the minor fault set, 36 of 125 faults) dip NE and SW. Despite the greater lengths and number of NE trending faults, individual faults from each of the two sets accrued similar maximum vertical displacements ranged up to ~700 ms for each stage (e.g., see Figures 10b and 10d).

Across the central ~190 km of the basin these displacements produced ~6–7% (~12–14 km extension) stretching in a NW-SE direction (Figure 9b; see locations of Traverse-2 and Traverse-3 in Figure 2) and ~2% (~3 km

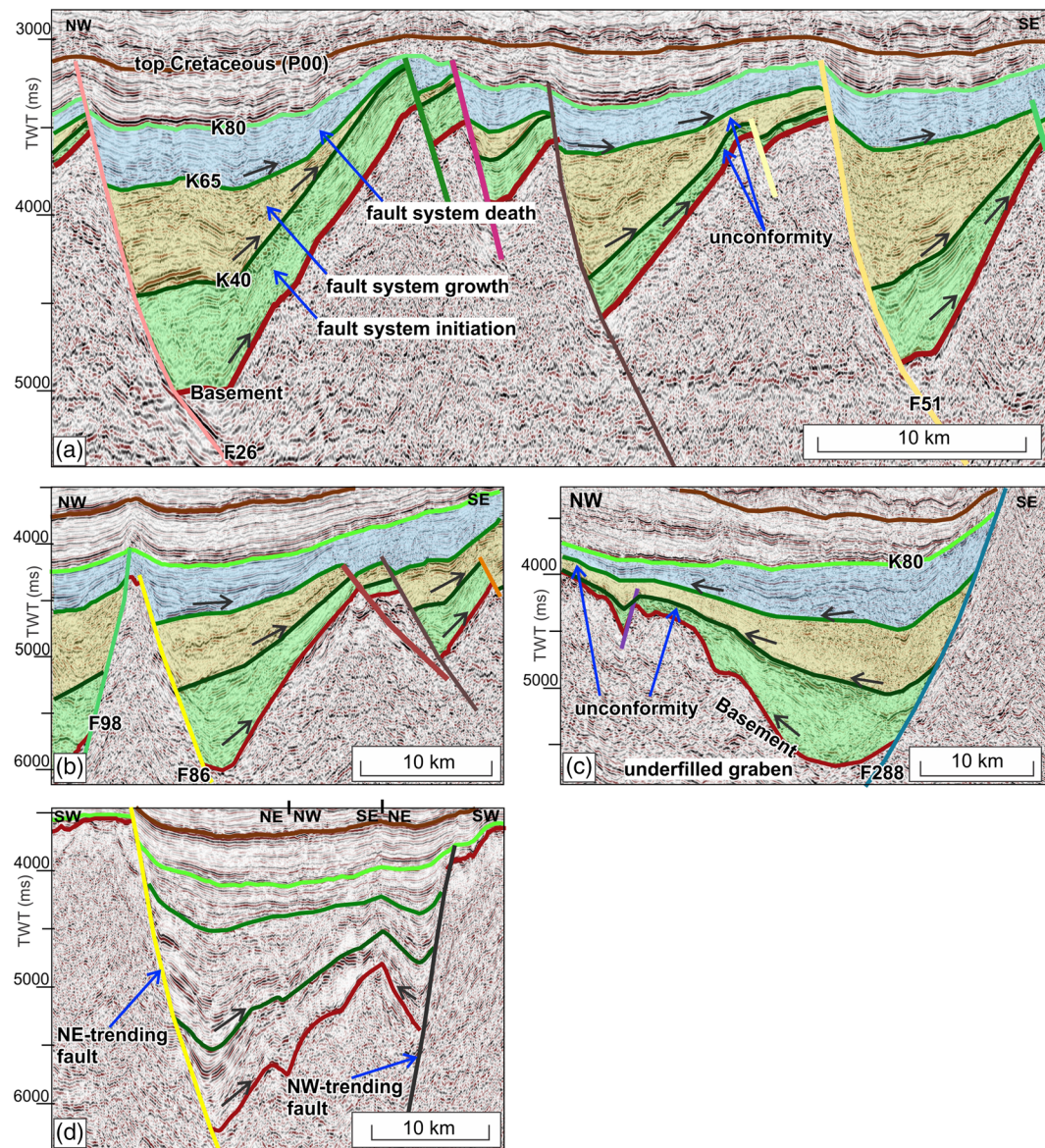


**Figure 8.** Seismic examples (a–c) showing three stages of faulting in the GSB. (d) Seismic example showing possible coeval activity of NE and NW trending faults. Each of the faulting stages show onlapping reflection packages (black arrows) and wedge-like reflection geometry. See Figure 2 for location of lines. Location of seismic lines in (d) are also shown in Figure 10.

extension) in a NE-SW direction (Figure 9b; see location of Traverse-5 in Figure 2). In contrast to the central region, there was negligible stretching in the southern and northern GSB (Figure 9b; see locations of Traverse-1 and Traverse-4 in Figure 2).

Normal faults and associated grabens active during this stage tend to cluster along two NW trends, parallel to the basement terrane boundaries exposed in the onshore South Island (Figure 7). In particular, faulting in Stage 1 is localized along the offshore projections of the southern boundary of the Murihiku Terrane and along the Dun Mountain-Maitai Terrane. These terrane boundaries appear to have formed planes of weakness that resulted in stress concentrations during the early stage of faulting in the GSB. These inferred locally elevated stresses may have partially reactivated preexisting basement terrane discontinuities, producing NW trending normal faults, and also resulted in the formation of new NE trending normal faults proximal to the terrane boundaries. The Horda platform in the Norwegian North Sea, where initiation of some faults at

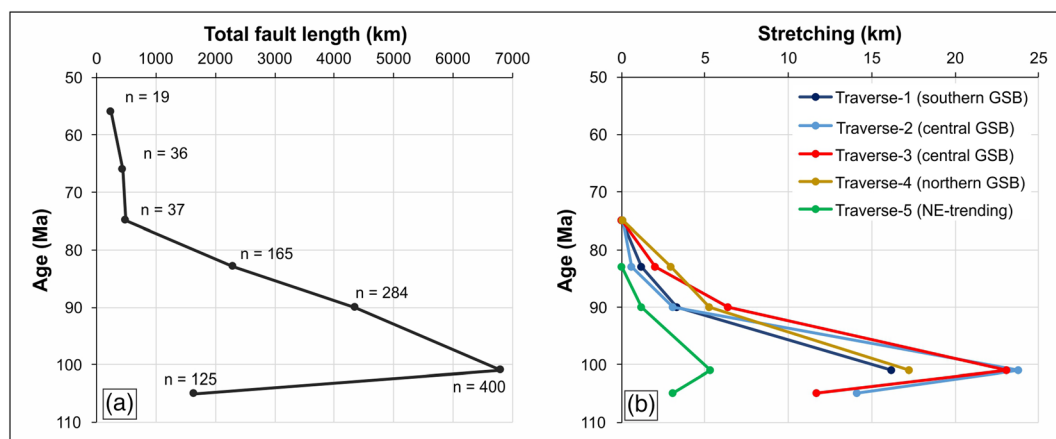


**Figure 9.** (a) Temporal variation of the total length of measured faults. (b) Variation of stretching through the Cretaceous. See Figure 2 for location of traverses.

preexisting structures have been reported, may provide an analogue for the basement structural controls in the GSB (Duffy et al., 2015). Synchronous displacement accumulation on NE and NW trending normal faults is interpreted to reflect local reorientation of stress fields close to the basement terrane boundaries. These inferred reorientations are locally associated with termination of NE trending faults along these boundaries (Figure 7a). Similar observations of inhibition of NE trending faults and rotation of faults are reported by Phillips and McCaffrey (2019) in a detailed study of faulting in the GSB-3D area (see location in Figure 2).

### 5.2. Stage 2—Fault System Growth

The second stage of faulting was characterized by an increase in the number, size (i.e. displacement and length) and areal extent of active faulting between ~101 and 90 Ma (Figures 6b and 7b). At ~101 Ma the total number of active faults and aggregate lengths of active faults increased to 400 ( $N = 125$  in Stage 1) and ~6,800 km (~1,650 km in Stage 1), respectively (Figure 9a). Two sets of fault orientations (NE and NW) accrued displacement during this stage (Figure 6b), although most of the active faults ( $N = 350$ ) and main grabens trended NE (Figure 7b). As with Stage 1 faulting, the majority of the NW trending faults during this stage were confined to the central GSB and localized along terrane boundaries, while NE trending faults were distributed across the basin. Displacements of up to 1,500 ms accumulated on NE trending faults (e.g., Faults F252, F280, and F288; see locations in Figure 10e) and up to 1,300 ms on NW trending faults (Fault, e.g., F340; Figure 10d) during this stage of faulting. Despite the similarity in maximum displacements between the two fault sets, the majority of faults with Stage 2 displacements >1,000 ms trended NE.

During the second stage of faulting NW-SE extension across the central GSB is ~12% (~23 km extension) and across the southern and northern GSB is ~8–9% (~16–18 km extension) (Figure 9b; see location of traverses in Figure 2), which is significantly higher than the amount of extension in the GSB during Stage 1. Extension along NE-SW direction was ~3% (~5 km extension), which primarily occurred in the central and northern GSB.

The lengths of faults and grabens active during Stage 2 varied from 5 to >100 km, with the longest faults generally present in the central and southern parts of the basin. The average fault length for Stage 2 was about ~17 km, which was slightly higher to the ~13 km in Stage 1. Fault lengths either remained the same (e.g., Figure 11b) or increased (e.g., Figure 11a) compared to the length of faults at Stage 1 extension. Some faults in the central basin that nucleated during Stage 1 appear to have established their lengths within the first 4 Myr of faulting (~105–101 Ma) with limited increases in length during the subsequent ~18 Myr (~101–83 Ma) of extension (Figure 11). This conclusion of early fault propagation followed by uniform fault lengths is consistent with the growth of other fault systems globally (e.g., Meyer et al., 2002; Nicol et al., 2020; Rotevatn et al., 2019; Walsh et al., 2002). However, similar to other global examples (Gillespie et al., 1992; Walsh & Watterson, 1988) the present work also suggests an outward migration of nucleation of individual faults associated with an increase in the areal extent of extension.

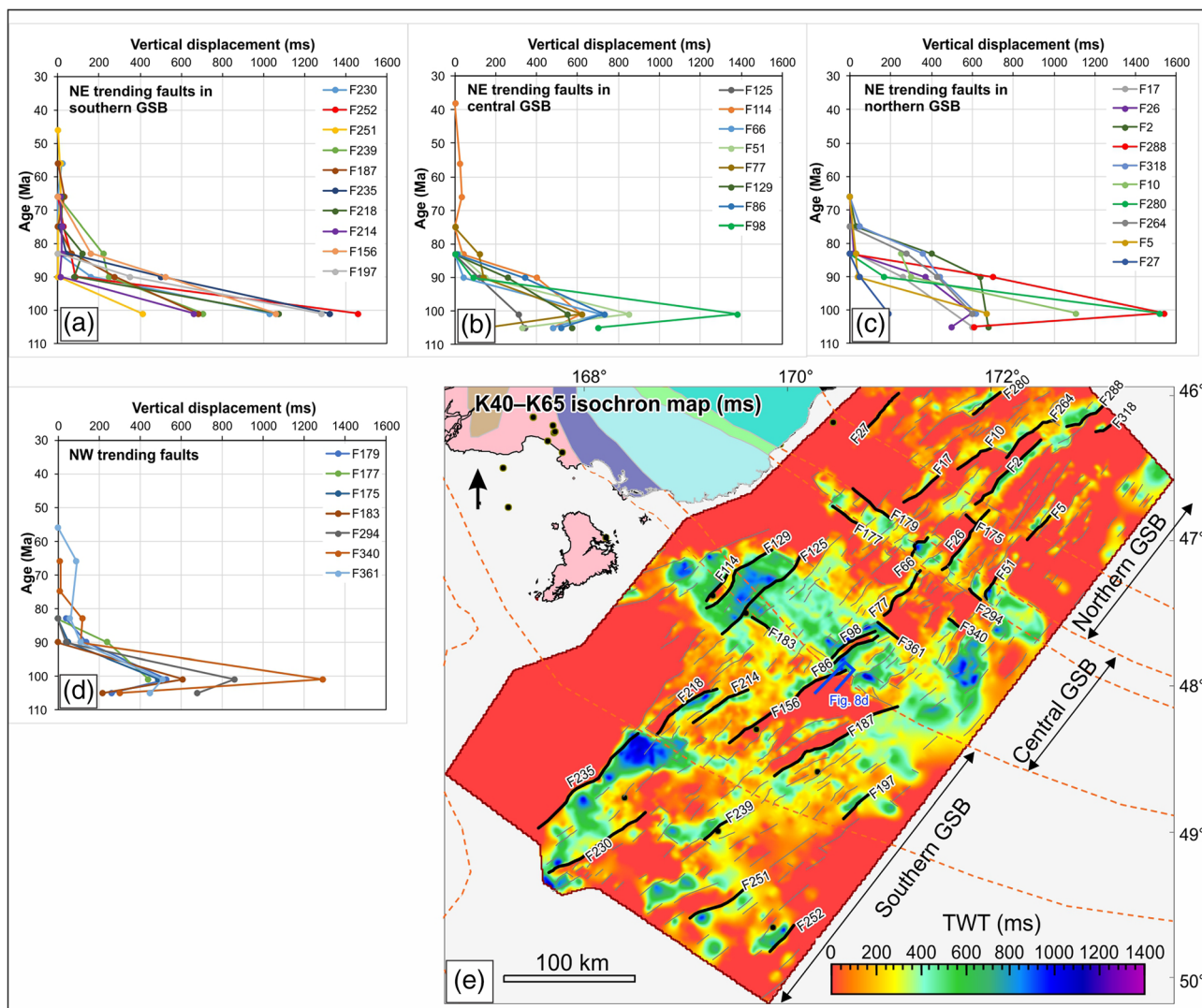


**Figure 10.** (a) Fault displacement profiles of 10 selected NE trending faults in the southern GSB region. (b) Fault displacement profiles of eight selected NE trending faults in the central GSB region. (c) Fault displacement profiles of 10 selected NE trending faults in the northern GSB region. (d) Fault displacement profiles of seven selected NW trending faults in the GSB. (e) Isochron map of K40-K65 interval showing the numbered faults used for fault displacement analysis.

Termination and bending of some NE trending faults at NW trending faults and/or along terrane boundaries are also observed for this stage of faulting. Bending of the southern tip of some of the NE trending faults occurs as they approach the southern margin of the Dun Mountain-Maitai Terrane and the boundaries of Median Batholith (Figure 7b). Bending of NE trending faults along the southern margin of the Median Batholith during this period of faulting has been reported by Phillips and McCaffrey (2019) and could reflect local reorientation of regional stress field at crustal-scale basement discontinuities (Fossen et al., 2016; Phillips & McCaffrey, 2019; Rotevatn et al., 2018).

### 5.3. Stage 3—Fault System Death

The third stage of faulting in the GSB occurred between 90–83 Ma and was characterized by a decrease in the number, lengths, and displacement rates of active faults compared to the second stage of faulting (Figures 6c and 6d, 7c and 7d, 9a, and 10). Faulting decreased throughout Stage 3 with a total of 284 faults and an aggregate fault length of ~4,350 km at ~90 Ma and 165 faults with a total length of ~2,300 km at ~83 Ma (Figure 9a). Two sets of fault orientations (NE and NW) were active during this stage (Figures 6c and 6d); however, most of the faults (258 of 284 at ~90 Ma and 158 of 165 at ~80 Ma) trended NE. The importance

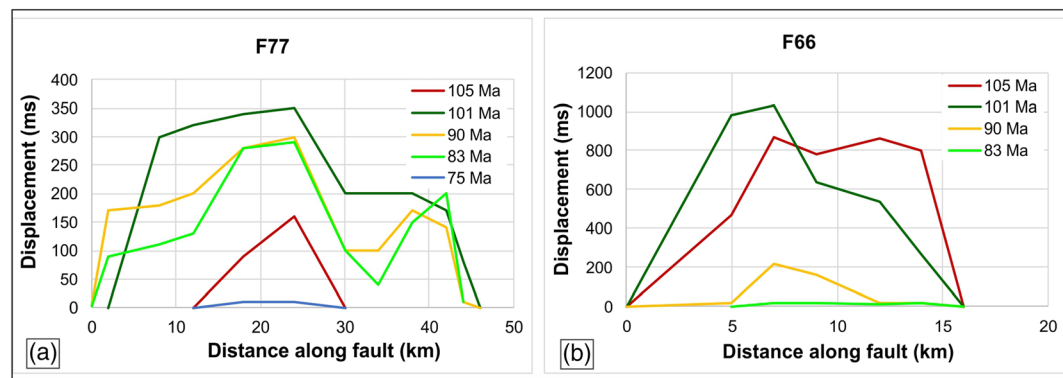


**Figure 11.** Examples showing vertical displacement of faults versus distance along fault trace of faults F77 (a) and F66 (b). See Figure 10 for location of faults.

of NW trending faults continued to decline with time. At the start of Stage 3 fewer NW trending faults were active than in Stage 2 ( $N = 26$  faults at  $\sim 90$  Ma and  $N = 7$  at  $\sim 83$  Ma compared to  $N = 50$  during Stage 2) and the displacements of NW trending faults continue to be generally smaller than NE trending faults. For example, on the  $\sim 90$  Ma horizon individual NE trending faults accommodate displacements of up to 700 ms, with the highest displacements in the northern GSB (Figure 10c), while NW trending faults show fault displacements up to 250 ms (Figure 10d). Fault displacements further decreased at  $\sim 83$  Ma with maximum displacements up to  $\sim 400$  ms along NE trending faults and  $\sim 100$  ms along NW trending faults. In Stage 3 the majority of NW trending faults continued to be located in the central GSB and localized along terrane boundaries, while NE trending faults were distributed over a wider area during this stage of extension. Similar to the previous stages of faulting, some of the NE trending faults terminate at, or swing in trend as they approach, basement terranes (Figure 7c).

The decline in the number of faults and their maximum displacements reflects a decrease in the rates of extension between Stages 2 and 3. In Stage 3 NW-SE extension across the GSB ranged from  $\sim 3\%$  ( $\sim 6$  km extension) in the central GSB to  $\sim 2\%$  ( $\sim 4$  km extension) in the southern and northern GSB (Figure 9b; see locations of Traverse-2 and Traverse-3 in Figure 2), which is significantly lower than  $\sim 23$  km extension observed during Stage 2. NE-SW extension at  $\sim 90$  Ma was negligible (<1% stretching). The observed decrease in extension together with the number and dimensions of active faults is indicative of fault system death, which appears to have commenced toward the end of Stage 2 faulting and was mostly complete by the end of Stage 3, a time interval of  $\sim 7$  Myr.

A small number of faults remained active after 83 Ma (Figures 6e and 6f), with some accruing minor displacements until the Eocene (Figure 10b). A total of 37 faults with total length of  $\sim 500$  km, 36 faults with an aggregate length of  $\sim 450$  km and 19 faults with an aggregate length of  $\sim 250$  km were interpreted at  $\sim 75$ , 66, and 56 Ma, respectively (Figure 9a). These faults were mainly oriented in NE with two minor faults oriented NW. Most of the faults at  $\sim 66$  and 56 Ma are located in the southern GSB region and fault displacements are  $<50$  ms. There was no clear evidence of fault-controlled growth strata and wedge-like depositional pattern observed post 83 Ma. Therefore, faulting post 83 Ma is considered as postrift faulting within the GSB. From  $\sim 83$  to 66 Ma the GSB formed a large depocenter (Figure 7d), which has been interpreted to reflect thermal sag of the lithosphere following Gondwana breakup (Constable & Crookbain, 2011; Sahoo, King, et al., 2014). The fault displacements post-83 Ma typically represent a small percentage of total displacement on the top basement horizon (e.g., <10%), and it remains possible that these displacements locally reflect sag of the lithosphere, differential compaction or polygonal faulting, which is widespread in Paleocene and Eocene strata (Bertoni et al., 2017; Sahoo, Seebeck, & Nicol, 2015).

## 6. Discussion

In broad terms rift evolution in the GSB was characterized by initial fault nucleation near to preexisting terrane boundaries, expansion of the fault system across the entire basin, and finally by death of fault system. In broad terms our rift evolution model is consistent with previously published two- and three-phase rift

models (Constable & Crookbain, 2011; Kirk & Constable, 2010; Kula et al., 2007; Tulloch et al., 2019). Although the precise timing of faulting and age of the rift phases/stages may differ slightly between publications, the primary difference between the models is that we believe the three stages of fault system evolution described here all predate Gondwana breakup rather than reflecting differences in the time that breakup commenced for different spreading centers (e.g., Kula et al., 2007; Tulloch et al., 2019). Early faulting (fault system initiation) was mainly developed in the central GSB with rift depocenters close to NW trending basement Murihiku and Dun Mountain-Maitai terrane boundaries. Numerous examples have been presented in the literature where the early nucleation and growth of faults is controlled by preexisting underlying discontinuities. Several workers have documented the geometric and spatial relationships between preexisting basement fabric and rift systems (Chattopadhyay & Chakra, 2013; Daly et al., 1989; McConnell, 1972; Morley, 1994, 1999a, 1999b; Morley et al., 2004; Phillips & McCaffrey, 2019; Rotevatn et al., 2018). Morley (1999b) described the strong influence of the preexisting fabric on the East African Rift Systems where rift faults are developed parallel to the fabric or oblique rift faults are develop along the fabric.

We cannot discount the possibility that some NW trending faults accommodated a strike-slip component of displacement; however, we suggest that NE and NW carry dominantly dip-slip. Analysis of growth strata adjacent to NW and NE trending faults and mapping of seismic horizons across the basin supports the view that NW and NE trending faults accommodated synchronous extension in two directions. For example, Figure 8d shows onlapping reflection patterns away from the faults and growth strata on footwall sides of the NE and NW trending faults. The similar thickness of growth strata in the early stage of faulting suggest coeval extension of both the NE and NW trending faults. Similar patterns of extension have been reported immediately north of the GSB in the Canterbury Basin where Barrier et al. (2020) attribute multidirectional extension to Gondwana breakup associated with the formation of variably oriented spreading centers, which might also account for the patterns of faulting in the GSB.

The importance of NW trending faults (compared to NE trending faults) decreased as the fault system evolved. With increasing regional extension in Stage 2 of faulting (fault system growth) the influence of basement fabric gradually decreased, while NE faults increased in number and spatial distribution. The increasing importance of the NE fault set appears to reflect the predominance of NW-SE extension, and the relative proximity of the GSB to the NE trending spreading center that now separates West Antarctica and Southern Zealandia. Stages 2 and 3 of faulting observed in the GSB are also observed across much of Zealandia continental crust (Figure 12), which subsequently separated from Australia and Antarctica (see Strogen et al., 2017, and references therein), suggesting that at this time the fault systems analyzed here covered an area much larger than the present study area. The large areal extent of extensional faulting at this time also supports the view that the faulting studied here developed in response to Gondwana breakup processes.

Many faults died in Stage 3 (fault system death) decreasing in length, number and displacement rates. Fault death is most noticeable for shorter faults (e.g., <25 km), which, in many cases, “switched off” during the ~90–83 Ma stage of faulting. By contrast, many of the longer faults remained active throughout this stage and some continued to accrue displacement following 83 Ma. The continued displacement of longer faults (at the expense of shorter faults) has been reported for normal faults globally where it is interpreted to reflect a strain localization process (Meyer et al., 2002). By contrast, in the GSB, strain localization associated with fault death accompanies a decrease in regional extension across the basin. Fault death is also associated with decreases in the lengths of some faults in the GSB (Figure 11), as was also observed by Meyer et al. (2002). NE trending faults (NW-SE extension) in the GSB are parallel to the Pacific-Antarctic spreading ridge that led to breakup of Southern Zealandia from West Antarctica and we suggest that this extension was primarily related to the distributed rifting of Zealandia during the embryonic phase of Gondwana breakup (Figures 6, 7, and 12). Similarly, it is also possible that extension on NW trending faults was related to separation along the NW trending spreading center between northern Zealandia and Australia/East Antarctica (Kula et al., 2007; Strogen et al., 2017). In the GSB the death of the fault system may primarily reflect a decrease in the stretching of the crust, which coincides with the formation of the spreading centers that resulted in the breakup of Gondwana. Thus, the death of the fault system may be related to the localization of far-field stretching on the rift margin. Extension across much of Zealandia occurred from ~105–83 Ma in regions including the Canterbury Basin, West Coast Basin, Taranaki Basin, Chatham Rise, and Southland Basin (Strogen et al., 2017, and references therein) (Figure 12) and supports a model in which crustal

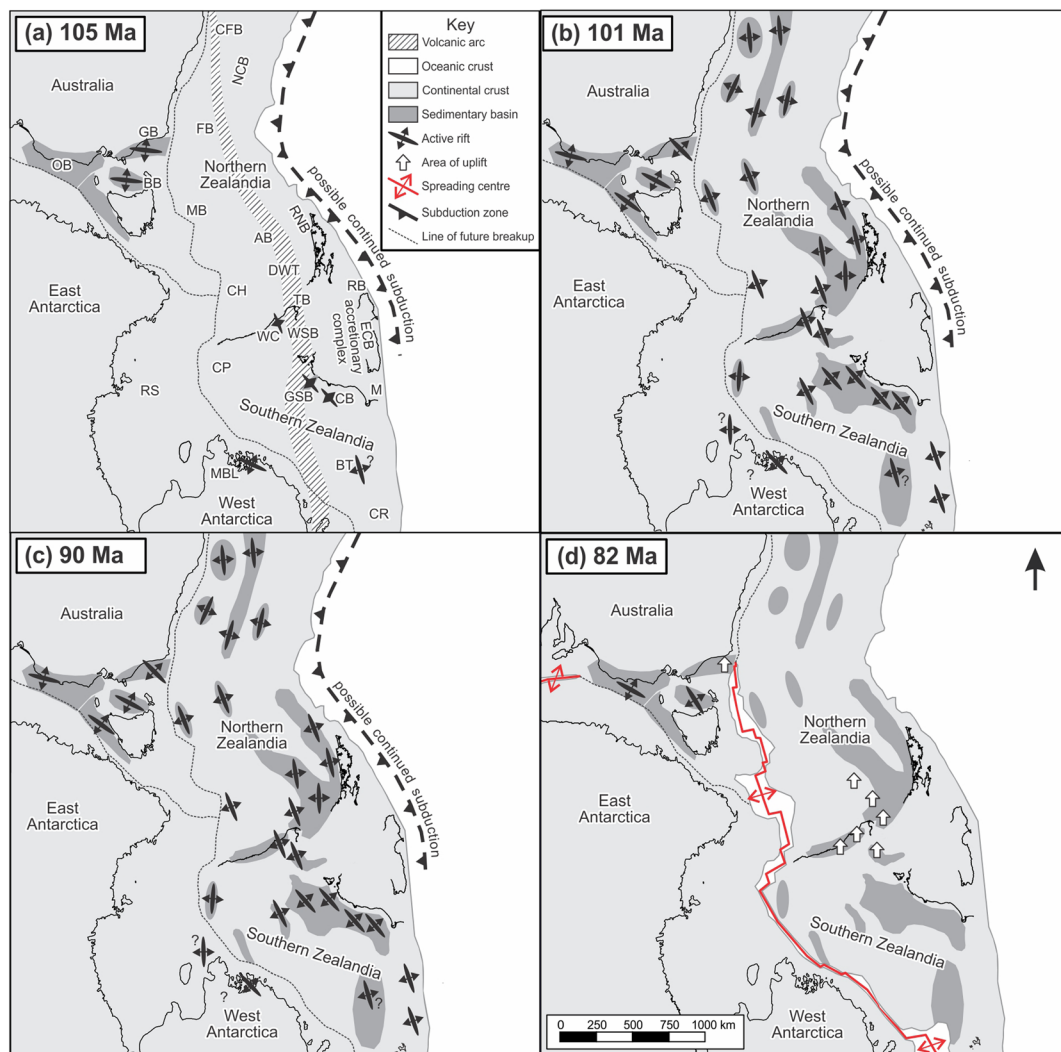


**Figure 12.** Tectonic reconstructions of the Antarctica-Zealandia-Australia region (modified after Strogen et al., 2017). (a) A map showing an initial stage of rifting (Stage 1) at ~105 Ma in GSB. The approximate future locations of sedimentary basins and position of volcanic arc are also shown. (b and c) Maps showing widespread Zealandia rifting in the GSB, CB, and other parts of Zealandia at ~101 and 90 Ma. (d) Approximately 82 Ma showing position of basins just after the end of rifting and initial seafloor spreading in the Southern Ocean and Tasman Sea. The 82 Ma is also associated with minor postrift related fault activity.

stretching is controlled by plate tectonic processes. We follow others in suggesting that the growth and death of rifting in the GSB and across the Zealandia continental crust reflects plate-scale localization of extension along spreading centers (Barrier, 2019; Barrier et al., 2020; Strogen et al., 2017).

## 7. Conclusions

Fault growth analysis in the Cretaceous succession has been performed on normal faults interpreted from seismic data in the GSB. They provide an improved understanding of Cretaceous rift evolution in the area with implications to other parts of Zealandia. The key results of this paper are as follows:

1. The majority of faults trend NE and primary stretching occurred along a NW-SE direction during rifting.
2. Three discrete stages of faulting have been recognized and are here referred to as; fault system initiation (Stage 1), fault system growth (Stage 2), and fault system death (Stage 3). Each stage records a different stage in the evolution of the fault system, which comprises dominant NE trending faults, and minor NW trending faults.

3. Stage 1 faulting (~105–101 Ma) mainly developed in the central GSB with rift depocenters close to NW trending basement terrane boundaries. These preexisting basement boundaries are interpreted to represent zones of weakness that locally promoted early localization of NW faulting and retarded the propagation of NE faulting.
4. Regional extension increased in Stage 2 (~101–90 Ma), and this increase was associated with a decrease in the influence of basement fabric. During Stage 2 NE trending faults increased in length, number, displacements, and spatial distribution.
5. Stage 3 (~90–83 Ma) was characterized by fault death with decreases in the length, number and displacements of faults. The cessation of faulting coincided with Gondwana breakup and reflects the localization of extension along spreading centers.

## Data Availability Statement

Seismic and well data used in this study were obtained from New Zealand Petroleum and Minerals (NZP&M) through the NZP&M 2018 data pack (<https://www.nzpam.govt.nz/maps-geoscience/petroleum-datapack/>).

## Acknowledgments

This work was supported by Strategic Science Investment Funding (SSIF) to the Sedimentary Basin Research and Te Riu-a-Maui/Understanding Zealandia programs and contestable funding (Atlas of Petroleum Prospectivity) from the New Zealand Government to GNS Science. We thank Paul Viskovic for his support on seismic data loading and Grant O'Brien for writing a python script to plot rose diagrams. Several colleagues have helped discuss technical aspects of the paper especially Glenn Thrasher, Andy Tulloch, Matt Sagar, and Andrea Barrier. We thank Kyle Bland, Glenn Thrasher, Thomas Phillips, and an anonymous reviewer for their constructive reviews that helped improve this manuscript and Jonathan Aitchison for his editorial handling of the paper. We thank Paradigm for providing software licenses for this study.

## References

- Adams, C. J., Campbell, H. J., Mortimer, N., & Griffin, W. L. (2017). Perspectives on Cretaceous Gondwana break-up from detrital zircon provenance of southern Zealandia sandstones. *Geological Magazine*, 154(4), 661–682. <https://doi.org/10.1017/S0016756816000285>
- Bache, F., Mortimer, N., Sutherland, R., Collot, J., Rouillard, P., Stagpoole, V., & Nicol, A. (2014). Seismic stratigraphic record of transition from Mesozoic subduction to continental breakup in the Zealandia sector of eastern Gondwana. *Gondwana Research*, 26(3–4), 1060–1078. <https://doi.org/10.1016/j.gr.2013.08.012>
- Barrier, A. (2019). Tectonics, sedimentation and magmatism of the Canterbury Basin, New Zealand. In *Chapter-2. The sedimentary fill of a Cretaceous under-filled syn-rift basin, Canterbury* (PhD thesis). Christchurch: University of Canterbury. Retrieved from <https://ir.canterbury.ac.nz/handle/10092/16809>
- Barrier, A., Nicol, A., Browne, G. H., Bassett, K., & Sahoo, T. (2018). An under-filled rift basin: Source, reservoir and seal distribution within the Canterbury Basin, New Zealand. Paper presented at AAPG ICE Conference, Cape Town, South Africa.
- Barrier, A., Nicol, A., Browne, G. H., & Bassett, K. N. (2020). Late Cretaceous coeval multi-directional extension in southeastern Zealandia: Implications for eastern Gondwana breakup. *Marine and Petroleum Geology*, 118, 104383. <https://doi.org/10.1016/j.marpetgeo.2020.104383>
- Beggs, J. M. (1993). Depositional and tectonic history of the Great South Basin. In P. F. Balance (Ed.), *South Pacific sedimentary basins, Sedimentary Basins of the World* (Vol. 2, pp. 365–373). Amsterdam: Elsevier science.
- Bertoni, C., Cartwright, J., Foschi, M., & Martin, J. (2017). Spectrum of gas migration phenomena across multi-layered sealing sequences. *AAPG Bulletin*, 102, 1011–1034.
- Blanke, S. (2015). PEP 38264 Caravel-1 well completion report. In *New Zealand Petroleum Report* (PR4896).
- Bradshaw, J. D. (1989). Cretaceous geotectonic patterns in the New Zealand region. *Tectonics*, 8(4), 803–820. <https://doi.org/10.1029/TC0081004p00803>
- Bull, S., Nicol, A., Strogen, D. P., Kroeger, K. F., & Seebeck, H. (2019). Tectonic controls on Miocene sedimentation in the Southern Taranaki Basin and implications for New Zealand plate boundary deformation. *Basin Research*, 31(2), 253–273. <https://doi.org/10.1111/bre.12319>
- CGGVeritas. (2009). Processing report GSB 3D. In *New Zealand Petroleum Report*, PR4055.
- Chattopadhyay, A., & Chakra, M. (2013). Influence of pre-existing pervasive fabrics on fault patterns during orthogonal and oblique rifting: An experimental approach. *Marine and Petroleum Geology*, 39, 74–91.
- Childs, C., Easton, S. J., Vendeville, B. C., Jackson, M. P. A., Lin, S. T., Walsh, J. J., & Watterson, J. (1993). Kinematic analysis of faults in a physical model of growth faulting above a viscous salt analogue. *Tectonophysics*, 228(3–4), 313–329. [https://doi.org/10.1016/0040-1951\(93\)90346-L](https://doi.org/10.1016/0040-1951(93)90346-L)
- Childs, C., Nicol, A., Walsh, J. J., & Watterson, J. (2003). The growth and propagation of synsedimentary faults. *Journal of Structural Geology*, 25, 633–648.
- Constable, R., & Crookbain, R. (2011). A sequences stratigraphic study of the Great South Basin. In *New Zealand Petroleum Report* (PR4348).
- Cook, R. A., Sutherland, R., & Zhu, H. (1999). *Cretaceous-Cenozoic geology and petroleum systems of the Great South basin, New Zealand, Institute of Geological and Nuclear Sciences Monograph* (Vol. 20, pp. 1–188). Lower Hutt: Institute of Geological and Nuclear Sciences.
- Cooper, A. F., Barreiro, B. A., Kimbrough, D. L., & Mattinson, J. M. (1987). Lamprophyre dyke intrusion and the age of the Alpine Fault, New Zealand. *Geology*, 15(10), 941–944. [https://doi.org/10.1130/0091-7613\(1987\)15<941:LDIATA>2.0.CO;2](https://doi.org/10.1130/0091-7613(1987)15<941:LDIATA>2.0.CO;2)
- Crampton, J. S., Mortimer, N., Bland, K. J., Strogen, D. P., Sagar, M., Hines, B. R., et al. (2019). Cretaceous termination of subduction at the Zealandia margin of Gondwana: The view from the paleo-trench. *Gondwana Research*, 70, 222–242. <https://doi.org/10.1016/j.gr.2019.01.010>
- Daly, M. C., Chorowicz, J., & Fairhead, D. (1989). Rift basin evolution in Africa: The influence of reactivated steep basement shear zones. In M. A. Cooper, & G. D. Williams (Eds.), *Inversion tectonics, Special Publication* (Vol. 44, pp. 309–334). London: Geological Society of London.
- Davison, I., & Underhill, J. R. (2012). Tectonics and sedimentation in extensional rifts: Implications for petroleum systems. In D. Gao (Ed.), *Tectonics and sedimentation: Implications for petroleum systems* (Vol. 100). Tulsa, OK: The American Association of Petroleum Geologists.
- Davy, B. (1993). The Bounty Trough—Basement structure influences on sedimentary basin evolution. In P. F. Ballance (Ed.), *South Pacific sedimentary basins, Sedimentary basins of the world 2* (pp. 69–92). Amsterdam: Elsevier science publishers.

- Davy, B. (2014). Rotation and offset of the Gondwana convergent margin in the New Zealand region following Cretaceous jamming of Hikurangi Plateau large igneous province subduction. *Tectonics*, 33, 1577–1595. <https://doi.org/10.1002/2014TC003629>
- Duffy, O. B., Bell, R. E., Jackson, C. A. L., Gawthorpe, R. L., & Whipp, P. S. (2015). Fault growth and interactions in a multiphase rift fault network: Horda platform, Norwegian North Sea. *Journal of Structural Geology*, 80, 99–119. <https://doi.org/10.1016/j.jsg.2015.08.015>
- Eagles, G., Gohl, K., & Larner, R. D. (2004). High-resolution animated tectonic reconstruction of the South Pacific and West Antarctic Margin. *Geochemistry, Geophysics, Geosystems*, 5, Q07002. <https://doi.org/10.1029/2003GC000657>
- Field, B. D., Browne, G. H., & Davy, B. W. (1989). Cretaceous and Cenozoic sedimentary basins and geological evolution of the Canterbury region, South Island, New Zealand. In *New Zealand Geological Survey basin studies* (Vol. 2, pp. 1–94).
- Fossen, H., Khani, H. F., Faleide, J. I., Ksienzyk, A. K., & Dunlap, W. J. (2016). Post-Caledonian extension in the West Norway–northern North Sea region: The role of structural inheritance. *Geological Society, London, Special Publications*, 439(1), 465–486. <https://doi.org/10.1144/SP439.6>
- Gaina, C., Müller, D. R., Royer, J. Y., Stock, J., Hardebeck, J., & Symonds, P. (1998). The tectonic history of the Tasman Sea: A puzzle with 13 pieces. *Journal of Geophysical Research*, 103(B6), 12,413–12,433. <https://doi.org/10.1029/98jb00386>
- Gawthorpe, R. L., & Leeder, M. R. (2000). Tectono-sedimentary evolution of active extensional basins. *Basin Research*, 12(3–4), 195–218. <https://doi.org/10.1046/j.1365-2117.2000.00121.x>
- Giba, M., Nicol, A., & Walsh, J. J. (2010). Evolution of faulting and volcanism in a backarc basin and its implications for subduction processes. *Tectonics*, 29, TC4020. <https://doi.org/10.1029/2009TC002634>
- Gillespie, P. A., Walsh, J. J., & Watterson, J. (1992). Limitations of dimensions and displacement data from single faults and the consequences for data analysis and interpretation. *Journal of Structural Geology*, 14(10), 1157–1172. [https://doi.org/10.1016/0191-8141\(92\)90067-7](https://doi.org/10.1016/0191-8141(92)90067-7)
- Grobys, J., Gohl, K., Davy, B., Uenzelmann-Neben, G., Deen, T., & Barker, D. (2007). Is the Bounty Trough off eastern New Zealand an aborted rift? *Journal of Geophysical Research*, 112, B03103. <https://doi.org/10.1029/2005JB004229>
- Grobys, J. W., Gohl, K., & Eagles, G. (2008). Quantitative tectonic reconstructions of Zealandia based on crustal thickness estimates. *Geochemistry, Geophysics, Geosystems*, 9, Q01005. <https://doi.org/10.1029/2007GC001691>
- Grobys, J. W., Gohl, K., Uenzelmann-Neben, G., Davy, B., & Barker, D. (2009). Extensional and magmatic nature of the Campbell Plateau and Great South basin from deep crustal studies. *Tectonophysics*, 472(1–4), 213–225. <https://doi.org/10.1016/j.tecto.2008.05.003>
- Hunt International Petroleum Co NZ. (1977a). Toroa-1 well completion report. In *New Zealand Petroleum Report*, PR691.
- Hunt International Petroleum Co NZ. (1977b). Final report Kawau-1A. In *New Zealand Petroleum Report*, PR716.
- Hunt International Petroleum Co NZ. (1977c). Pakaha-1 well completion report. In *New Zealand Petroleum Report*, PR703.
- Hunt International Petroleum Co NZ. (1978a). Hoiho-1C well completion report. In *New Zealand Petroleum Report*, PR730.
- Hunt International Petroleum Co NZ. (1978b). Tara-1 well completion report. In *New Zealand Petroleum Report*, PR732.
- Hunt International Petroleum Co NZ. (1978c). Takapu-1 & Takapu-1A well completion report. In *New Zealand Petroleum Report*, PR733.
- King, P., & Thrasher, G. (1996). *Cretaceous-Cenozoic geology and petroleum systems of the Taranaki Basin, New Zealand* (Vol. 13, pp. 1–243). Institute of Geological and Nuclear Sciences Ltd.
- Kirk, R., & Constable, R. (2010). Seismic facies mapping and paleogeographic interpretation from seismic sequence stratigraphy. In *New Zealand Petroleum Report* (PR4347).
- Kula, J., Tulloch, A. J., Spell, T. L., & Wells, M. L. (2007). Two-stage rifting of Zealandia-Australia-Antarctica: Evidence from  $^{40}\text{Ar}/^{39}\text{Ar}$  thermochronometry of the Sisters Shear Zone, Stewart Island, New Zealand. *Geology*, 35(5), 411–414. <https://doi.org/10.1130/G23432A.1>
- Kula, J., Tulloch, A. J., Spell, T. L., Wells, M. L., & Zanetti, K. (2009). Thermal evolution of the Sisters Shear Zone, southern New Zealand: Formation of the Great South Basin and onset of Pacific-Antarctic spreading. *Tectonics*, 28, TC5015. <https://doi.org/10.1029/2008TC002368>
- Laird, M. G. (1993). Cretaceous continental rifts: New Zealand region. In P. F. Ballance (Ed.), *South Pacific sedimentary basins, Sedimentary basins of the world* (Vol. 2, pp. 37–49). Amsterdam: Elsevier science.
- Laird, M. G., & Bradshaw, J. D. (2004). The break-up of a long-term relationship: The Cretaceous separation of New Zealand from Gondwana. *Gondwana Research*, 7(1), 273–286. [https://doi.org/10.1016/S1342-937X\(05\)70325-7](https://doi.org/10.1016/S1342-937X(05)70325-7)
- Luyendyk, B. P. (1995). Hypothesis for cretaceous rifting of East Gondwana caused by subducted slab capture. *Geology*, 23(4), 373–376. [https://doi.org/10.1130/0091-7613\(1995\)023<0373:HFCROE>2.3.CO;2](https://doi.org/10.1130/0091-7613(1995)023<0373:HFCROE>2.3.CO;2)
- Luyendyk, B. P., Cisowski, S., Smith, C. H., Richard, S. M., & Kimbrough, D. L. (1996). Paleomagnetic study of the northern Ford Ranges, western Marie Byrd Land, West Antarctica: A middle Cretaceous pole, and motion between West and East Antarctica? *Tectonics*, 15, 122–141.
- Luyendyk, B. P., Wilson, D. S., & Siddoway, C. S. (2003). Eastern margin of the Ross Sea rift in western Marie Byrd Land, Antarctica: Crustal structure and tectonic development. *Geochemistry, Geophysics, Geosystems*, 4(10), 1090. <https://doi.org/10.1029/2002GC000462>
- McConnell, R. B. (1972). Geological development of the rift system of eastern Africa. *Geological Society of America Bulletin*, 83(9), 2549–2572. [https://doi.org/10.1130/0016-7606\(1972\)83\[2549:GDOTRS\]2.0.CO;2](https://doi.org/10.1130/0016-7606(1972)83[2549:GDOTRS]2.0.CO;2)
- Meyer, V., Nicol, A., Childs, C., Walsh, J. J., & Watterson, J. (2002). Progressive localisation of strain during the evolution of a normal fault population. *Journal of Structural Geology*, 24(8), 1215–1231. [https://doi.org/10.1016/S0191-8141\(01\)00104-3](https://doi.org/10.1016/S0191-8141(01)00104-3)
- Morley, C. K. (1994). Structural geology of rifts. In J. J. Lambiase (Ed.), *Hydrocarbon habitat in rift basins* (Vol. 80, pp. 75–102). London: Geological Society Special Publication.
- Morley, C. K. (1999a). How successful are analogue models in addressing the influence of pre-existing fabrics on rift structures? *Journal of Structural Geology*, 21(8–9), 1267–1274. [https://doi.org/10.1016/S0191-8141\(99\)00075-9](https://doi.org/10.1016/S0191-8141(99)00075-9)
- Morley, C. K. (1999b). Influence of pre-existing fabrics on rift structure. In C. K. Morley (Ed.), *Geoscience of rift systems—Evolution of East Africa, AAPG Studies in Geology* (Vol. 44, pp. 151–160). Tulsa, OK: The American Association of Petroleum Geologists.
- Morley, C. K., Haranaya, C., Phoosongsee, W., Pongwapee, S., Kornsawan, A., & Wonganan, N. (2004). Activation of rift oblique and rift parallel pre-existing fabrics during extension and their effect on deformation style: Examples from the rifts of Thailand. *Journal of Structural Geology*, 26(10), 1803–1829. <https://doi.org/10.1016/j.jsg.2004.02.014>
- Mortimer, N. (2004). New Zealand's geological foundations. *Gondwana Research*, 7, 261–272.
- Mortimer, N., Campbell, H. J., Tulloch, A., King, P., Stagpoole, V., Wood, R., et al. (2017). Zealandia: Earth's hidden continent. *GSA Today*, 27(3), 27–35. <https://doi.org/10.1130/GSATG32IA.1>
- Mortimer, N., Davey, F. J., Melhuish, A., Yu, J., & Godfrey, N. J. (2002). Geological interpretation of a deep seismic reflection profile across the Eastern Province and Median Batholith, New Zealand: Crustal architecture of an extended Phanerozoic convergent orogen. *New Zealand Journal of Geology and Geophysics*, 45(3), 349–363. <https://doi.org/10.1080/00288306.2002.9514978>

- Mortimer, N., McLaren, S., & Dunlap, W. J. (2012). Ar-Ar dating of K-feldspar in low grade metamorphic rocks: Example of an exhumed Mesozoic accretionary wedge and forearc, South Island, New Zealand. *Tectonics*, 31, TC3020. <https://doi.org/10.1029/2011TC003057>
- Mortimer, N., Rattenbury, M. S., King, P. R., Bland, K. J., Barrell, D. J. A., Bache, F., et al. (2014). High-level stratigraphic scheme for New Zealand rocks. *New Zealand Journal of Geology and Geophysics*, 57(4), 402–419. <https://doi.org/10.1080/00288306.2014.946062>
- Mortimer, N., Tulloch, A. J., Spark, R. N., Walker, N. W., Ladley, E., Allibone, A., & Kimbrough, D. L. (1999). Overview of the Median Batholith, New Zealand: A new interpretation of the geology of the Median Tectonic Zone and adjacent rocks. *Journal of African Earth Sciences*, 29(1), 257–268. [https://doi.org/10.1016/S0899-5362\(99\)00095-0](https://doi.org/10.1016/S0899-5362(99)00095-0)
- Mortimer, N., van den Bogaard, P., Hoernle, K., Timm, C., Gans, P., Werner, R., & Rieftahl, F. (2019). Late Cretaceous oceanic plate reorganization and the breakup of Zealandia and Gondwana. *Gondwana Research*, 65, 31–42. <https://doi.org/10.1016/j.gr.2018.07.010>
- Muir, R. J., Bradshaw, J. D., Weaver, S. D., & Laird, M. G. (2000). The influence of basement structure on the evolution of the Taranaki Basin, New Zealand. *Journal of the Geological Society*, 157(6), 1179–1185. <http://doi.org/10.1144/jgs.157.6.1179>
- Muir, R. J., Ireland, T. R., Weaver, S. D., & Bradshaw, J. D. (1994). Ion microprobe U-Pb zircon geochronology of granitic magmatism in the Western Province of the South Island, New Zealand. *Chemical Geology*, 113(1–2), 171–189. [https://doi.org/10.1016/0009-2541\(94\)90011-6](https://doi.org/10.1016/0009-2541(94)90011-6)
- Muir, R. J., Weaver, S. D., Bradshaw, J. D., Eby, G. N., & Evans, J. A. (1995). The Cretaceous Separation Point batholith, New Zealand: Granitoid magmas formed by melting of mafic lithosphere. *Journal of the Geological Society*, 152, 689–701.
- Nicol, A., Mazengarb, C., Chanier, F., Rait, G., & Uruski, C. (2007). Tectonic evolution of the active Hikurangi Subduction margin, New Zealand, since the Oligocene. *Tectonics*, 26, TC4002. <https://doi.org/10.1029/2006TC002090>
- Nicol, A., Walsh, J. J., Childs, C., & Manzocchi, T. (2020). The growth of faults. Chapter 6. In D. Tanner, & C. Brandes (Eds.), *Understanding faults: Detecting, dating, and modelling* (pp. 221–256). New York: Elsevier.
- Phillips, T. B., & McCaffrey, K. J. W. (2019). Terrane boundary reactivation, barriers to lateral fault propagation and reactivated fabrics: Rifting across the median batholith zone, great South Basin, New Zealand. *Tectonics*, 38, 4027–4053. <https://doi.org/10.1029/2019TC005772>
- Placid Oil Company. (1984a). Well report, Rakiura-1, Great South Basin, New Zealand. In *New Zealand Petroleum Report*, PR994.
- Placid Oil Company. (1984b). Final geological well completion report, Pukaki-1, Great South Basin, New Zealand, PPL38081. In *New Zealand Petroleum Report*, PR1005.
- Raine, J. I., Kennedy, E. M., Griffin, A. G., Sykes, R., & Clowes, C. D. (2018). *Materials for improved assessment of the petroleum source potential of New Zealand coal-rich rocks, 1: Mid-Cretaceous stratigraphy, coal abundance, flora and climate* (GNS Science Report, 2018/07, pp. 1–99).
- Ravnås, R., & Steel, R. J. (1998). Architecture of marine rift-basin successions. *AAPG Bulletin*, 82(1), 110–146.
- Reilly, C., Nicol, A., Walsh, J. J., & Seebeck, H. (2015). Evolution of faulting and plate boundary deformation in the Southern Taranaki Basin, New Zealand. *Tectonophysics*, 651–652, 1–18. <https://doi.org/10.1016/j.tecto.2015.02.009>
- Rotevatn, A., Jackson, C. A. L., Tvedt, A. B. M., Bell, R. E., & Blækkan, I. (2019). How do normal faults grow? *Journal of Structural Geology*, 125, 174–184. <https://doi.org/10.1016/j.jsg.2018.08.005>
- Rotevatn, A., Kristensen, T. B., Ksienzyk, A. K., Wemmer, K., Henstra, G. A., Midtkandal, I., et al. (2018). Structural inheritance and rapid rift-length establishment in a multiphase rift: The east Greenland rift system and its Caledonian orogenic ancestry. *Tectonics*, 37, 1858–1875. <http://doi.org/10.1029/2018TC005018>
- Sahoo, T. R., & Bland, K. J. (compilers). (2017). *Atlas of petroleum prospectivity, Southeast Province: ArcGIS geodatabase and technical report, GNS Science Data Series 23c* (pp. 1–53). Retrieved from <https://data.gns.cri.nz/pbe/index.html?menu=APP>
- Sahoo, T. R., Browne, G. H., & Hill, M. G. (2014). Seismic attribute analysis and depositional elements in the Canterbury Basin. In: Advantage NZ, Geotechnical Petroleum Forum 2014, 1–3 April 2014.
- Sahoo, T. R., King, P. R., Bland, K. J., Strogen, D. P., Sykes, R., & Bache, F. (2014). Tectono-sedimentary evolution and source rock distribution of the mid to Late Cretaceous succession in the Great South Basin, New Zealand. *APPEA Journal*, 54(1), 259–274. <https://doi.org/10.1071/AJ13026>
- Sahoo, T. R., Kroeger, K. F., Thrasher, G., Munday, S., Mingard, H., Cozens, N., & Hill, M. P. (2015). Facies distribution and impact on petroleum migration in the Canterbury Basin, New Zealand. In *Eastern Australian basins symposium 2015: Publication of proceedings* (pp. 187–202). Petroleum Exploration Society of Australia: Perth, WA.
- Sahoo, T. R., Seebeck, H., & Nicol, A. (2015). Polygonal fault systems in the Canterbury Basin, New Zealand. In: Advantage NZ, Geotechnical Petroleum Forum 2015, 1–3 April 2015.
- Schiøler, P., Browne, G. H., Cameron, H., King, P. R., Strogen, D. P., Sahoo, T., & Funnell, R. H. (2017). Great South Basin: National wells audit pilot project play analysis report, GNS Science Consultancy Report 2017/20. In *New Zealand Petroleum Report* (PR5428, pp. 1–70).
- Schiøler, P., & Raine, J. I. (2009). Palynology of lower Hoiho Group in the Great South Basin and Clipper and Horse Range Formations in the Canterbury Basin, GNS Science Consultancy Report, 2009/361. In *New Zealand Petroleum Report* (PR4348, pp. 1–67).
- Schiøler, P., Raine, J. I., Crundwell, M. P., Fohrmann, M., Griffin, A., Hollis, C. J., et al. (2012). Revised biostratigraphy and well correlation, Canterbury Basin, New Zealand; updated with results from Cutter-1 well. GNS Science Consultancy Report, 2012/248, 164 p. in *New Zealand Petroleum Report*, PR4621.
- Schiøler, P., Raine, J. I., Crundwell, M. P., Griffin, A., Hollis, C. J., Kulhanek, D. K., et al. (2011). Revised biostratigraphy and well correlation, Canterbury Basin, New Zealand, GNS Science Consultancy Report 2011/12. In *New Zealand Petroleum Report* (PR4365, pp. 1–142).
- Scott, J., & Cooper, A. J. T. (2006). Early Cretaceous extensional exhumation of the lower crust of a magmatic arc: Evidence from the Mount Irene shear zone, Fiordland, New Zealand. *Tectonics*, 25, TC2018. <https://doi.org/10.1029/2005TC001890>
- Shell GSB Ltd. (2013). Great South Basin seismic data processing report. In *New Zealand Petroleum Report*, PR4758.
- Siddoway, C. S., Baldwin, S. L., Fitzgerald, P. G., Fanning, C. M., & Luyendyk, B. P. (2004). Ross Sea mylonites and the timing of intra-continental extension within the West Antarctic rift system. *Geology*, 32, 57–60.
- Spell, T., McDougall, I., & Tulloch, A. J. (2000). Thermochronologic constraints on the breakup of the Pacific Gondwana margin: The Paparoa Metamorphic Core Complex, South Island, New Zealand. *Tectonics*, 19(3), 433–451. <https://doi.org/10.1029/1999TC900046>
- Strogen, D. P., & King, P. R. (2014). A new Zealandia-wide seismic horizon naming scheme. *GNS Science Report*, 2014/34 (pp. 1–20).
- Strogen, D. P., Seebeck, H., Nicol, A., & King, P. R. (2017). Two-phase Cretaceous–Paleocene rifting in the Taranaki Basin region, New Zealand: Implications for Gondwana break-up. *Journal of the Geological Society*, 174(5), 929–946. <https://doi.org/10.1144/jgs2016-160>
- Sutherland, R. (1995). The Australia-Pacific boundary and Cenozoic plate motions in the SW Pacific: Some constraints from Geosat data. *Tectonics*, 14(4), 819–831. <https://doi.org/10.1029/95TC00930>

- Sutherland, R., King, P. R., & Wood, R. A. (2001). Tectonic evolution of Cretaceous rift basins in south-eastern Australia and New Zealand: Implications for exploration risk assessment. In K. C. Hill, & T. Bernecker (Eds.), *Eastern Australasian basins symposium 2001* (pp. 3–13). Melbourne: Petroleum Exploration Society of Australia.
- Tarling, M. S., Smith, S. A. F., Scott, J. M., Rooney, J. S., Viti, C., & Gordon, K. C. (2019). The internal structure and composition of a plate-boundary-scale serpentinite shear zone: The Livingstone Fault, New Zealand. *Solid Earth*, 10(4), 1025–1047. <https://doi.org/10.5194/se-10-1025-2019>
- Taylor, S. K., Nicol, A., & Walsh, J. J. (2008). Displacement loss on growth faults due to sediment compaction. *Journal of Structural Geology*, 30(3), 394–405. <https://doi.org/10.1016/j.jsg.2007.11.006>
- Tulloch, A. (2010). Detrital zircon U-Pb geochronology and provenance from 13 sandstone samples from seven Great South Basin wells. In *New Zealand Petroleum Report* (4219, pp. 1–275).
- Tulloch, A. J., & Kimbrough, D. L. (2003). Paired plutonic belts in convergent margins and the development of high Sr/Y magmatism: The Peninsular Ranges Batholith of California and the Median Batholith of New Zealand. *Geological Society of America Special Papers*, 374, 275–295.
- Tulloch, A. J., Mortimer, N., Ireland, T. R., Waught, T. E., Maas, R., Palin, J. M., et al. (2019). Reconnaissance basement geology and tectonics of South Zealandia. *Tectonics*, 38, 516–551. <https://doi.org/10.1029/2018TC005116>
- Tulloch, A. J., Ramezani, J., Kimbrough, D. L., Faure, K., & Allibone, A. H. (2009). U-Pb geochronology of mid-Paleozoic plutonism in western New Zealand: Implications for S-type granite generation and growth of the East Gondwana margin. *Geological Society of America Bulletin*, 121(9–10), 1236–1261. <https://doi.org/10.1130/B26272.1>
- Uruski, C. I., Kennedy, C., Harrison, T., Maslen, G., Cook, R. A., Sutherland, R., & Zhu, H. (2007). Petroleum potential of the Great South Basin, New Zealand—New seismic data improves imaging. *APPEA Journal*, 47(1), 143–160.
- Walsh, J. J., Nicol, A., & Childs, C. (2002). An alternative model for the growth of faults. *Journal of Structural Geology*, 24(11), 1669–1675. [https://doi.org/10.1016/S0191-8141\(01\)00165-1](https://doi.org/10.1016/S0191-8141(01)00165-1)
- Walsh, J. J., & Watterson, J. (1988). Analysis of the relationship between displacements and dimensions of faults. *Journal of Structural Geology*, 10(3), 239–247. [https://doi.org/10.1016/0191-8141\(88\)90057-0](https://doi.org/10.1016/0191-8141(88)90057-0)
- Walsh, J. J., Watterson, J., & Yielding, G. (1991). The importance of small-scale faulting in regional extension. *Nature*, 351, 391–393.